Highly Efficient Catalysts in Directed Oxygen-Transfer Processes: Synthesis, Structures of Novel Manganese-Containing Heteropolyanions, and Applications in Regioselective Epoxidation of Dienes with Hydrogen Peroxide

Michael Bösing, Andreas Nöh, Ina Loose, and Bernt Krebs*

Contribution from the Anorganisch-Chemisches Institut der Universität, Wilhelm-Klemm-Strasse 8, D-48149 Münster, Germany

Received December 17, 1997

Abstract: A series of novel manganese(II)-substituted polyoxometalates, $[(Mn^{II}(H_2O)_3)_2(WO_2)_2(BiW_9O_{33})_2]^{10-}$ (**1**), $[(Mn^{II}(H_2O))_3(SbW_9O_{33})_2]^{12-}$ (**2**), and $[(Mn^{II}(H_2O)_3)_2(Mn^{II}(H_2O)_2)_2(TeW_9O_{33})_2]^{8-}$ (**3**), were synthesized and characterized by X-ray structure analyses. The use of these oxidatively and solvolytically stable heteropolyanions as homogeneous catalysts for the epoxidation of dienes was investigated by gas chromatography/mass spectrometry, IR spectroscopy, UV−visible studies, and cyclic voltammetric measurements. The catalytic performance is exemplified by the model substrate (*R*)-(+)-limonene, at ambient temperatures in a biphasic system, with excellent regioselectivities, >99%, and very high turnovers even with only a small molar excess of hydrogen peroxide.

Introduction

Selective oxidation of organic compounds has been extensively studied and is still subject of high interest.[1−7] One major goal in this field of research is the replacement of stoichiometric oxidation processes by catalytic oxygen transfer reactions as in the epoxidation of unsaturated hydrocarbons (eq 1). A further

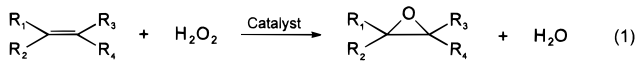

(1)

intention is the synthesis of custom-made, effective, and nontoxic catalysts to achieve lowering of costs and environmentally friendly conditions in industrial processes. Generally, important prerequisites for these technologies are stable catalysts with high product selectivities and reaction rates at ambient temperatures without waste of the applied oxidant. Consequently, one of the preferred solutions for these problems is to use inorganic and therefore robust transition metal substituted complexes as catalysts in combination with hydrogen peroxide as an oxygen donor.

At present, heteropolymetalates, especially with low-valent transition metals such as manganese(II), cobalt(II), iron(II), and ruthenium(III), have been shown to be efficient for catalytic oxygen-transfer reactions as in the epoxidation of alkenes.[8−13] Usually, the active sites in these complexes are located at the heteroatoms substituted into a deficient polyoxometalate deriving from the well-known Keggin structure as an inorganic ligand.[14,15] A good example for remarkably high catalytic potential in hydrogen peroxide mediated oxidations is the heteropolyanion $[WZnMn^{II}_2(ZnW_9O_{34})_2]^{12-}$. This compound has been reported to be an effective catalyst with high product selectivities producing epoxides from dialkyl- and trialkyl-substituted olefins (cyclooctene and 2-methyl-2-heptene) with high turnover numbers.[16,17] Other more or less efficient compounds have been described in the literature.[18−20] Nevertheless, up to now catalytic epoxidation using transition metal substituted polyoxometalates (TMSPs) is limited to alkenes containing one double bond, with one exception where a manganese(III)-substituted heteropolyanion, $[\alpha_2\text{-}MnBrP_2W_{17}O_{61}]^{8-}$, catalyzes the oxidation of a diene,

* Corresponding author. Fax: +251/8338366. E-mail: krebs@uni-muenster.de.

(1) Sheldon, R. A.; Kochi, J. K. *Metal-Catalyzed Oxidations of Organic Compounds*; Academic Press: New York, 1981; Chapter 3.
(2) Parshall, G. W.; Ittel, S. D. *Homogeneous Catalysis: The Applications and Chemistry of Catalysis by Soluble Transition Metal Complexes*, 2nd ed.; Wiley-Interscience: New York, 1992; pp 151−261.
(3) Sheldon, R. A. In *Dioxygen Activation and Homogeneous Catalytic Oxidation*; Simandi, L. I., Ed.; Elsevier: Amsterdam, 1991; pp 573−594.
(4) Sheldon, R. A. *ChemTech* **1991**, *21*, 566−576.
(5) Jørgensen, K. A. *Chem. Rev.* **1989**, *89*, 431−458.
(6) Jørgensen, K. A.; Schiøtt, B. *Chem. Rev.* **1990**, *90*, 1483−1506.
(7) Grinstaff, M. W.; Hill, M. G.; Labinger, J. A.; Gray, H. B. *Science* **1994**, *264*, 1311−1313.
(8) Hill, C. L.; Brown, R. B., Jr. *J. Am. Chem. Soc.* **1986**, *108*, 536−539.
(9) Loose, I.; Bösing, M.; Klein, R.; Krebs, B.; Schulz, R. P.; Scharbert, B. *Inorg. Chim. Acta* **1997**, *263*, 99−108.
(10) Hill, C. L.; Zhang, X. *Nature* **1995**, *373*, 324−326.
(11) Zhang, X.; Sasaki, K.; Hill, C. L. *J. Am. Chem. Soc.* **1996**, *118*, 4809−4816.
(12) Khenkin, A. M.; Hill, C. L. *Mendeleev Commun.* **1993**, 140−142.
(13) Neumann, R.; Abu-Gnim, C. *J. Am. Chem. Soc.* **1990**, *112*, 6025−6031.
(14) Pope, M. T. *Heteropoly and Isopoly Oxometalates*; Springer: Berlin, 1983.
(15) Pope, M. T.; Müller A. *Angew. Chem., Int. Ed. Engl.* **1991**, *30*, 34−48.
(16) Neumann, R.; Gara, M. *J. Am. Chem. Soc.* **1995**, *117*, 5066−5074.
(17) Reaction conditions. (a) Epoxidation of cyclooctene: substrate/oxidant (30% H_2O_2)/catalyst = 5000/10 000/1, 2 °C, 24 ⇒ 1465 turnovers to cyclooctene oxide. (b) Epoxidation of 2-methyl-2-heptene: substrate/oxidant (30% H_2O_2)/catalyst = 5000/10 000/1, 22 °C, 20 ⇒ 2300 turnovers to 2-methyl-2-heptene oxide.
(18) Khenkin, A. M.; Hill, C. L. *J. Am. Chem. Soc.* **1993**, *115*, 8178−8186.
(19) Duncan, D. C.; Chambers, C.; Hecht, E.; Hill, C. L. *J. Am. Chem. Soc.* **1995**, *117*, 681−691.
(20) Hill, C. L.; Prosser-McCartha, C. M. *Coord. Chem. Rev.* **1995**, *143*, 407−455 and references therein.

S0002-7863(97)04281-9 CCC: $15.00
Published on Web 07/03/1998

Table 1. Crystal Structure Data of Compounds Containing the Anions $[(Mn^{II}(H_2O)_3)_2(WO_2)_2(BiW_9O_{33})_2]^{10-}$ (**1**), $[(Mn^{II}(H_2O))_3(SbW_9O_{33})_2]^{12-}$ (**2**), and $[(Mn^{II}(H_2O)_3)_2(Mn^{II}(H_2O)_2)_2(TeW_9O_{33})_2]^{8-}$ (**3**)

	$Na_6(NH_4)_4$[**1**]·$37H_2O$	$Na_{11}(NH_4)$[**2**]·$45H_2O$	Na_8[**3**]·$34H_2O$
formula	$H_{102}N_4O_{113}Na_6Mn_2Bi_2W_{20}$	$H_{100}NO_{114}Na_{11}Mn_3Sb_2W_{18}$	$H_{84}O_{108}Na_8Mn_4Te_2W_{18}$
formula weight (M), g mol^{-1}	6309.64	5909.32	5780.85
crystal size, mm^3	0.15 × 0.12 × 0.25	0.10 × 0.25 × 0.35	0.10 × 0.075 × 0.125
crystal color/habit	yellow needles	red plates	yellow needles
crystal system	monoclinic	monoclinic	monoclinic
space group	$P2_1/n$ (no. 14)	$C2/c$ (no. 15)	$P2_1/n$ (no. 14)
a, Å	12.850(3)	14.209(3)	12.456(2)
b, Å	25.100(5)	23.336(5)	12.812(3)
c, Å	16.020(3)	32.334(6)	29.579(6)
α, deg	90	90	90
β, deg	95.08(3)	99.08(3)	100.67(3)
γ, deg	90	90	90
V, Å^3	5147(2)	10587(4)	4639(2)
Z	2	4	2
ρ_{calcd}, g cm^{-3}	4.07	3.707	4.139
μ, mm^{-1}	26.04	20.484	23.527
F(000)	5592	10596	5144
T, K	153	293	193
2θ range	$4° < 2\theta < 48°$	$4° < 2\theta < 48°$	$9° < 2\theta < 52°$
no. of indep reflns	8090	7673	9015
no. of reflns obsd ($>2\sigma(I)$)	5632	6532	7341
no. of variables	392	394	372
GOF on F^2	1.072	1.069	1.043
R ($>2\sigma(I)$)	$R_1{}^a = 0.0789$	$R_1{}^a = 0.0826$	$R_1{}^a = 0.0455$
	$wR_2{}^b = 0.1594$	$wR_2{}^b = 0.2189$	$wR_2{}^b = 0.1000$
R (all data)	$R_1{}^a = 0.1247$	$R_1{}^a = 0.0935$	$R_1{}^a = 0.0606$
	$wR_2{}^b = 0.2042$	$wR_2{}^b = 0.2345$	$wR_2{}^b = 0.1071$
$(\Delta/\rho)_{max}$, e$^-$/Å^3	4.509	4.460	2.761
$(\Delta/\rho)_{min}$, e$^-$/Å^3	−3.371	−4.240	−1.792

[a] $R_1 = \sum||F_o| - |F_c||/\sum|F_o|$. [b] $wR_2 = [\sum w(F_o^2 - F_c^2)^2/\sum w(F_0^4)]^{1/2}$. $w_1 = 1/[\sigma^2(F_o^2) + (0.055P)^2 + 1100.2224P]$. $w_2 = 1/[\sigma^2(F_o^2) + (0.1333P)^2 + 1445.7198P]$. $w_3 = 1/[\sigma^2(F_o^2) + (0.0406P)^2 + 105.035P]$. $P = (F_o^2 + 2F_c^2)/3$.

(*R*)-(+)-limonene, with PhIO.[21] In this reaction, also relatively high turnovers are obtained and a good (but not quantitative) regioselectivity of 1,2-limonene oxide:8,9-limonene oxide (2.4:1) is found.[22]

Epoxidations of (*R*)-(+)-limonene with species of the non-TMSP Ishii−Venturello system ($H_3[PW_{12}O_{40}]$·xH_2O/H_2O_2/PTC) lead to 90−100% conversion to 1,2-limonene oxide;[23] nevertheless these systems work stoichiometrically and diepoxides have been produced either.

Other previously reported catalysts for regioselective alkene epoxidation are various metalloporphyrins.[24] For example, (*R*)-(+)-limonene was oxidized in benzene with aqueous NaOCl using manganese porphyrins with varying steric demands to give different regioselectivities. The ratio of external epoxide to ring epoxide is 0.22 for an unhindered porphyrin and 1.63 for the most hindered porphyrin.

However, comparing all known polyoxometalates used as catalysts in epoxidation reactions, one common feature can be realized: None of them meets all the important requirements including stability, high product selectivity, high turnovers at ambient temperatures, applicability with environmentally friendly oxidants, and high regioselectivity.

We now report the use of novel oxidatively and solvolytically stable manganese-substituted heteropolyanions, $[(Mn^{II}(H_2O)_3)_2(WO_2)_2(BiW_9O_{33})_2]^{10-}$ (**1**), $[(Mn^{II}(H_2O))_3(SbW_9O_{33})_2]^{12-}$ (**2**), and $[(Mn^{II}(H_2O)_3)_2(Mn^{II}(H_2O)_2)_2(TeW_9O_{33})_2]^{8-}$ (**3**), as catalysts for the epoxidation of dienes. Each applied catalyst was characterized by X-ray structure analysis. In a biphasic system at ambient temperatures, (*R*)-(+)-limonene was taken as model substrate leading to excellent regioselectivities, >99%, and very high turnovers even with only a small molar excess of hydrogen peroxide.

Experimental Section

Crystal Structure Determination. Diffraction experiments were performed on a SYNTEX $P2_1$ diffractometer (for **1**) and a STOE IPDS imaging plate system (for **2** and **3**), respectively, with Mo Kα radiation (λ = 0.710 73 Å) and with corrections for absorption (using XEMP, ellipsoid correction (for **1**), DECAY (for **2**), and DECAY/ABSCOR (for **3**)). The structures were solved by direct methods using SHELXL-PLUS and refined with SHELXL 93 (on F^2) by full-matrix least squares. Oxygen atoms were refined isotropically, all other atoms (excluding poorly ordered sodium atoms) were refined anisotropically. As usual for polyoxometalates, the three crystal structures show large disorder in the range of counterions and water molecules. Accordingly, the exact formulas were determined by elemental analyses. Details of the crystal data collection and processing and structure analysis and refinement for **1**−**3** are summarized in Table 1. Tables of positional and thermal parameters and thermal ellipsoid figures are presented in the Supporting Information.

Syntheses of the Catalysts. $[(Mn^{II}(H_2O)_3)_2(WO_2)_2(BiW_9O_{33})_2]^{10-}$ (1). Na_2WO_4·$2H_2O$ (4.40 g, 13.34 mmol) was dissolved in a mixture of water (20 mL) and concentrated HNO_3 (15.67 M, 0.7 mL) and heated to 75 °C (solution 1). $BiONO_3$·H_2O (0.4 g, 1.34 mmol) was dissolved in concentrated HNO_3 (15.67 M, 0.7 mL), heated to 75 °C, and carefully treated with water (10 mL) (solution 2). The bismuth-containing solution 2 was added dropwise to solution 1, and Na_2CO_3 (0.4 g, 4.8 mmol) was supplied simultaneously to avoid a drop in pH. To this pale yellow mixture was given slowly a solution of $MnCl_2$·$4H_2O$ (0.266 g, 1.34 mmol) in water (10 mL), leading to a deep yellow solution.

(21) Mansuy, D.; Bartoli, J.-F.; Battiono, P.; Lyon, D. K.; Finke, R. G. *J. Am. Chem. Soc.* **1991**, *113*, 7222−7226.

(22) Reaction conditions: substrate/oxidant (PhIO)/catalyst = 500/10/1, 20 °C, 2 h fi 7.5 turnovers to 1,2-limonene oxide (mixture of cis and trans isomers) based upon starting PhIO, ratio 1,2-limonene oxide:8,9-limonene oxide = 2.4:1.

(23) Salles, L.; Aubry, C.; Thouvenot, R.; Robert, F.; Dorémieux-Morin, C.; Chottard, G.; Ledon, H.; Jeannin, Y.; Brégeault, J.-M. *Inorg. Chem.* **1994**, 33, 871−878. Herein a catalytic test for the epoxidation of (*R*)-(+)-limonene by using the ($H_3[PW_{12}O_{40}]$·xH_2O/H_2O_2/PTC) system was performed.

(24) Suslick, K. S. In *Activation and Functionalization of Alkanes*; Hill, C. L., Ed.; Wiley: New York, 1989; pp 219−241.

Using a concentrated HNO_3 solution (15.67 M) the pH was set to 5−6. After heating and stirring for 1 h at 75 °C, the mixture was allowed to cool to ambient temperature. Finally, NH_4NO_3 (0.534 g, 6.67 mmol) was added to the reaction solution and yellow needles of $Na_6(NH_4)_4[(Mn^{II}(H_2O)_3)_2(WO_2)_2(BiW_9O_{33})_2]\cdot 37H_2O$ were obtained after several hours. Yield: 2.4 g (57%). Anal. Calcd for $H_{102}N_4O_{113}Na_6Mn_2Bi_2W_{20}$: H, 1.62; N, 0.89; Na, 2.19; Mn, 1.74; Bi, 6.62; W, 58.26; H_2O, 12.27. Found: H, 1.51; N, 0.97; Na, 2.11; Mn, 1.98; Bi, 6.74; W, 58.11; H_2O, 12.49.

$[(Mn^{II}(H_2O))_3(SbW_9O_{33})_2]^{12-}$ (2). The first step in synthesis of **2** is the preparation of $Na_9[SbW_9O_{33}]\cdot 19.5H_2O$.[25] This compound was prepared by the reaction of $Na_2WO_4\cdot 2H_2O$ (40 g, 121 mmol) in boiling water (80 mL) and dropwise addition of Sb_2O_3 (1.96 g, 6.72 mmol) dissolved in concentrated HCl (12 M, 10 mL). The mixture was refluxed for 1 h and was allowed to cool slowly. Colorless crystals of $Na_9[SbW_9O_{33}]\cdot 19.5H_2O$ were formed after evaporation of one-third of the solution volume. Yield: 28.0 g (72%). In a second step, $Na_9[SbW_9O_{33}]\cdot 19.5H_2O$ (4 g 1.4 mmol) was dissolved in water (8 mL) under gentle heating. To this pale yellow mixture was given slowly a solution of $MnCl_2\cdot 4H_2O$ (0.414 g, 2.08 mmol) in water (10 mL), leading to an orange solution with pH 6−7. The mixture was refluxed for 1 h, and then NH_4NO_3 (0.673 g, 8.4 mmol) was added. After the mixture was cooled to ambient temperature, dark orange crystals of $Na_{11}(NH_4)[(Mn^{II}(H_2O))_3(SbW_9O_{33})_2]\cdot 45H_2O$ were obtained after several days. Yield: 2.6 g (63%). Anal. Calcd for $H_{100}NO_{114}Na_{11}Mn_3Sb_2W_{18}$: H, 1.70; N, 0.24; Na, 4.28; Mn, 2.78; Sb, 4.12; W, 55.99; H_2O, 14.62. Found: H, 1.51; N, 0.35; Na, 4.35; Mn, 2.83; Sb, 4.25; W, 55,81; H_2O, 14.71.

$[(Mn^{II}(H_2O)_3)_2(Mn^{II}(H_2O)_2)_2(TeW_9O_{33})_2]^{8-}$ (3). TeO_2 (0.22 g, 1.34 mmol) was dissolved under gentle heating in concentrated NaOH solution (ca. 10 M, 1 mL) and diluted with water (10 mL) (solution 1). $Na_2WO_4\cdot 2H_2O$ (3.96 g, 12.01 mmol) was dissolved in a mixture of water (20 mL) and concentrated HNO_3 (12 M, 0.7 mL) and heated to 75 °C (solution 2). The tellurium-containing solution 1 was added dropwise to solution 2, and Na_2CO_3 (0.4 g, 4.8 mmol) was supplied simultaneously to avoid a drop in pH. To this pale yellow mixture a solution of $MnCl_2\cdot 4H_2O$ (0.532 g, 2.68 mmol) in water (10 mL) was given slowly leading to a deep yellow solution. The pH was set to 3 by dropwise addition of a concentrated HNO_3 solution (15.67 M). After heating and stirring for 1 h at 80 °C the mixture was filtered and allowed to cool to ambient temperature. Yellow crystals of $Na_8[(Mn^{II}(H_2O)_3)_2(Mn^{II}(H_2O)_2)_2(TeW_9O_{33})_2]\cdot 34H_2O$ were obtained after several days. Yield: 1.8 g (47%). Anal. Calcd for $H_{84}O_{108}Na_8Mn_4Te_2W_{18}$: H, 1.45; Na, 3.18; Mn, 3.80; Te, 4.41; W, 57.23; H_2O, 13.70. Found: H, 1.53; Na, 2.98; Mn, 3.71; Te, 4.53; W, 57.37; H_2O, 14.01.

Catalytic Epoxidation Procedure. Stock solutions were prepared by dissolving $Na_6(NH_4)_4$[**1**]$\cdot 37H_2O$, $Na_{11}(NH_4)$[**2**]$\cdot 45H_2O$ or Na_8[**3**]$\cdot 34H_2O$ (0.064 mmol) and methyltricaprylammonium chloride (0.64 mmol (**1**), 0.77 (**2**), and 0.52 (**3**)) in a water/1,2-dichloroethane mixture (20 mL, 1:1 ratio). Under gentle heating and stirring, the color of the organic phase turned to yellow (**1** and **3**) and orange (**2**), respectively, whereas the aqueous phase decolorized. The organic solution was separated and cooled. In a typical reaction, the substrate, (*R*)-(+)-limonene, (40 mmol) and desired amounts of the stock solution were dissolved in 1,2-dichloroethane (40 mL) at room temperature. The reaction was initiated by addition of 30% hydrogen peroxide (Fluka, purum p.a., stab., with phosphate (PO_4) ≤ 0.0002%, 80 mmol) under atmospheric conditions and stirred, forming a biphasic system. Due to the biphasic reaction system, product rates are a function of interfacial area and so almost equal stirring rates (800−1000 rpm) and identical reaction vessels were used. The epoxidation process was monitored by gas chromatography; aliquots were taken from the organic phase of the reaction medium (after quenching the reaction by demixing of the organic and aqueous phase) and directly injected into the gas chromatograph (Finnigan MAT DANI 8521 equipped with a ITD 800 mass-selective detector with a CP-SIL-8CB column and GC Hewlett-Packard 6890 equipped with a mass-selective detector HP 5973 with fused silica column, respectively) to identify and quantify the organic products by integration of peak areas; *p*-cymene was used as an internal standard.

(25) Bösing, M.; Loose, I.; Pohlmann, H.; Krebs, B. *Chem. Eur. J.* **1997**, *3*, 1232−1237.

Analysis Data of the Organic Products. The organic products were identified by mass spectroscopy at 70 eV. **II**: *m*/*z* (%) 152 (1.1), 137 (13.9), 119 (6.8), 109 (16.2), 93 (19.5), 79 (27.4), 71 (8.5), 67 (52.6), 53 (15.8), 43 (100.0), 39 (76.3). **III**: *m*/*z* (%) 152 (<1), 137 (2.1), 119 (2.4), 108 (14.7), 93 (25.7), 79 (36.4), 67 (47.5), 53 (15.7), 43 (100.0), 39 (71.1). **IV**: *m*/*z* (%) 152 (5.4), 137 (7.0), 134 (1.7), 123 (3.7), 108 (9.6), 97 (3.7) 93 (10.1), 88 (4.8), 82 (7.3), 79 (7.0), 71 (44.8), 67 (32.4), 57 (18.6), 43 (100.0), 41 (42.3). In addition to this, chemical ionization (CI) experiments with methanol as the reaction gas were performed to verify the 152 *m*/*z* molecule peaks of **II**−**IV**. In all cases the $(M + H)^+$ peak (153 *m*/*z*) was found.

Identification of the organic products by ^1H NMR was done on a Bruker 300-MHz spectrometer ($CDCl_3$). **II**: δ (ppm) 1.27 (s, 3H), 1.67 (s, 3H), 2.98 (t, 1H), 4.66 (s, 2H), 1.15−2.20 (m, 7H, ring protons). **III**: δ (ppm) 1.29 (s, 3H), 1.71 (s, 3H), 3.02 (t, 1H), 4.75 (s, 2H), 1.13−2.27 (m, 7H; ring protons). **IV**: δ (ppm) 1.20 (s, 3H), 1.66 (s, 3H), 1.86 (ddd, 1H) 3.56 (s, broad, 1H (OH)), 4.67 (s, 2H), 1.41−1.80 (m, 6H; ring protons).

UV−Visible Studies. Examination of the UV−vis spectra of $[Mn^{II}_2(H_2O)_6(WO_2)_2(BiW_9O_{33})_2]$,[10−] $[(Mn^{II}(H_2O))_3(SbW_9O_{33})_2]^{12-}$, and $[(Mn^{II}(H_2O)_3)_2(Mn^{II}(H_2O)_2)_2(TeW_9O_{33})_2]^{8-}$ was performed on a Hewlett-Packard 8453 diode array spectrophotometer:

First measurements (400−800 nm, under reaction conditions, substrate/catalyst = 1000/1, yellow (**1** and **3**) and orange (**2**) solutions, partial evaporation of the solvent) showed no peaks in the spectra on the basis of the 2+ oxidation states of the manganese atoms in the catalysts before reaction.

In further investigations (400−800 nm, under reaction conditions, substrate/catalyst = 1000/1, after addition of 2 equiv of 30% aqueous hydrogen peroxide based upon the substrate and stirring, after ca. 40 h, red color depending on the 3+ oxidation states of at least one manganese atom in the catalysts, partial evaporation of the solvent) distinctive peaks at 490 nm (**1**), 498 nm (**2**), and 514 nm (**3**) were formed during the reactions. Several days after completion of the epoxidations, the color of the mixtures changed slowly to yellow (**1** and **3**) and orange (**2**) again based on the 2+ oxidation states of the manganese atoms in the catalysts leading to the original spectra of $[Mn^{II}_2(H_2O)_6(WO_2)_2(BiW_9O_{33})_2]^{10-}$, $[(Mn^{II}(H_2O))_3(SbW_9O_{33})_2]^{12-}$, and $[(Mn^{II}(H_2O)_3)_2(Mn^{II}(H_2O)_2)_2(TeW_9O_{33})_2]^{8-}$.

Measurements in the 200−400-nm range of diluted solutions of **1**−**3** used in the experiments described before showed a distinctive peak at 227 nm and a shoulder at ca. 270 nm. The spectrum of the quaternary ammonium salt methyltricaprylammonium chloride in 1,2-dichloroethane (5×10^{-3} M) contained two distinctive peaks at 227 and 273 nm.

Cyclic Voltammetric Measurements. Electrochemical experiments were performed with a BAS CV-50 W appliance. Measurements of **1**−**3** were made in 1,2-dichloroethane solutions (1×10^{-3} M, 10 mL) containing tetra-*n*-butylammonium perchlorate (0.342 g, 1 mmol) as the supporting electrolyte and were conducted at room temperature under an argon atmosphere. A controlled growth mercury working electrode (Metrohm) and an Ag/AgCl reference electrode were used for the experiments. Effective redox potentials of $[Mn^{II}Mn^{III}HPA]^+$−$[Mn^{III}Mn^{III}HPA]^{2+}$ and $[Mn^{II}Mn^{II}HPA]$−$[Mn^{II}Mn^{III}HPA]^+$: $E_{1/2}$ (mV) = ca. 640 and ca. 275 (**1**), ca. 480 and ca. 10 (**2**), ca. 840 (irreversible process) and ca. 485 (**3**) with DE (mV) = ca. 90 and ca. 110 (**1**), ca. 100 and ca. 180 (**2**), and ca. 75 (**3**). Redox potentials corresponding to the formation of $[Mn^{II}Mn^{II}HPA]^{-/2-}$: $E_{1/2}$ (mV) = ca. −80 (**1**), ca. −130 (**2**), and ca. −140 and −580 (irreversible process) (**3**) with DE (mV) = ca. 60 (**1**), ca. 140 (**2**), and ca. 160 (**3**). All redox potentials were determined from an average of the anodic and cathodic peak potentials from various measurements. Voltage sweep rates were 750 mV/s (**1**), 250 mV/s (**2**), and 200 mV/s (**3**).

Infrared Spectroscopy. IR spectra of $Na_6(NH_4)_4[Mn_2(H_2O)_6(WO_2)_2(BiW_9O_{33})_2]\cdot 37H_2O$, $Na_{11}(NH_4)[(Mn^{II}(H_2O))_3(SbW_9O_{33})_2]\cdot 45H_2O$, and $Na_8[(Mn^{II}(H_2O)_3)_2(Mn^{II}(H_2O)_2)_2(TeW_9O_{33})_2]\cdot 34H_2O$ were taken on a Perkin-Elmer 683 spectrometer in a range 4000 −400 cm^{-1}. Sodium ammonium salt of **1** (KBr): $\tilde{\nu}$ (cm^{-1}) = 937 (vs) (W−O_t); 818 (vs) (W−O_c−W); 760 (s) (W−O_e−W); 669 (s). Sodium ammonium salt

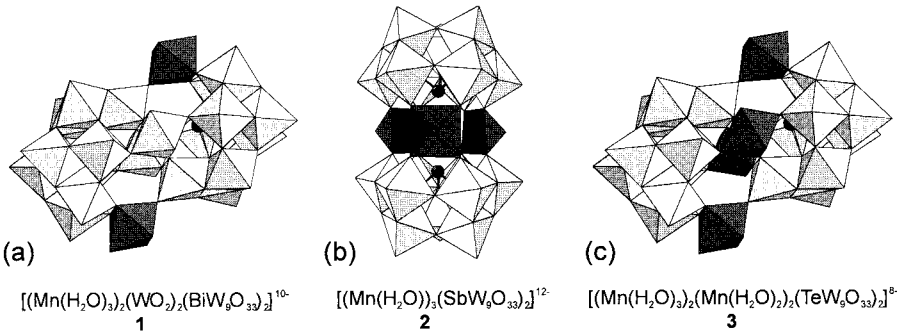

Figure 1. Polyhedron plot of the molecular structures of $[(Mn^{II}(H_2O)_3)_2(WO_2)_2(BiW_9O_{33})_2]^{10-}$ (**1**), $[(Mn^{II}(H_2O))_3(SbW_9O_{33})_2]^{12-}$ (**2**), and $[(Mn^{II}(H_2O)_3)_2(Mn^{II}(H_2O)_2)_2(TeW_9O_{33})_2]^{8-}$ (**3**). Bi^{III}, Sb^{III}, and Te^{IV} heteroatoms are shown as black balls in the clusters of the XW_9 units forming the catalysts. Mn^{II} ions are within the darker octahedra, and the bright octahedra represent the WO_6 units.

of **2** (KBr): $\tilde{\nu}$ (cm^{-1}) = 934 (vs) (W−O_t); 865 (vs) (W−O_c−W); 772 (s) (W−O_e−W); 719 (vs). Sodium salt of **3** (KBr): $\tilde{\nu}$ (cm^{-1}) = 970 (s) (W−O_t); 847 (vs) (W−O_c−W); 791 (vs) (W−O_e−W); 672 (s).

IR spectra of the catalysts after interaction with aqueous hydrogen peroxide were taken of powders obtained from typical reaction mixtures (several days after completion of the epoxidations, yellow (**1** and **3**) and orange (**2**) solutions based on the restoration of the anions to their original forms) by evaporating the solvent. Compound containing **1** (KBr): $\tilde{\nu}$ (cm^{-1}) = 939 (vs) (W−O_t); 859 (vs) (W−O_c−W); 762 (s) (W−O_e−W); 669 (s). Compound containing **2** (KBr): $\tilde{\nu}$ (cm^{-1}) = 936 (vs) (W−O_t); 866 (vs) (W−O_c−W); 768 (s) (W−O_e−W); 717 (vs). Compound containing **3** (KBr): $\tilde{\nu}$ (cm^{-1}) = 965 (s) (W−O_t); 836 (vs) (W−O_c−W); 785 (vs) (W−O_e−W); 673 (s) (t, terminal; c, corner-sharing; e, edge-sharing).

Results and Discussion

Structural Characterization of the Catalysts. Like many other polyoxometalates, **1**−**3** contain isomeric fragments of the well-known α-Keggin structure connected to each other by manganese(II) ions in a different way. A new type of these sandwich complexes of the general formula $[M_2(H_2O)_6(WO_2)_2(XW_9O_{33})_2]^{(14-2n)-}$, M^{n+} = Fe^{3+}, Co^{2+}, Mn^{2+}, Ni^{2+}, Zn^{2+}, and X = Sb^{III} can be synthesized by a novel strategy reported by us earlier.[25] Using this procedure, **1** was obtained by substitution of the desired manganese(II) ion into a $[(WO_2)_4(OH)_2(BiW_9O_{33})_2]^{12-}$ precursor compound. **2** and **3** were obtained by application of the same strategy using manganese(II) ions and $[SbW_9O_{33}]^{9-}$ and the in situ precursor $[TeW_9O_{33}]^{8-}$, respectively.

In particular, the X-ray structure analysis of the mixed sodium ammonium salt $Na_6(NH_4)_4$[**1**]·$37H_2O$ (Table 1) reveals a novel polyoxometalate composed of two identical β-B-$[BiW_9O_{33}]^{9-}$ fragments joined together by two corner-sharing WO_6 octahedra and two octahedral $Mn^{II}O_3(H_2O)_3$ groups. Both manganese atoms are bonded through two oxygen atoms of one unit and one oxygen atom of the other unit to the tungsten−oxygen framework with an average Mn−O_W bond length of 2.07 Å. A view of the anion is shown in Figure 1a. The lacunary tungsten cage of each β-B-BiW_9 subunit consists of three corner-sharing W_3O_{13} groups with centered Bi^{III} atoms which are pyramidally surrounded by three oxygen atoms with an average Bi−O_{W3Bi} bond length of 2.11 Å. The lone electron pair is located on the top of this pyramid. Generally, β-B-$[XW_9O_{33}]^{n-}$ units can be derived from the α-B-type anions by 60° rotation of one W_3O_{13} group around the X−O_{W3X} binding vector. Special features of this cluster are the existence of WO_6 octahedra without any terminal oxygen atoms and the presence of three free coordination sites at the manganese atoms which are completed by water molecules. Mn−O_{H2} bond lengths are observed between 2.15(3) and 2.19(3) Å. Selected bond lengths and angles of **1** are presented in Table 2.

Table 2. Bond Lengths (Å) and Angles (deg) of the Anions $[(Mn^{II}(H_2O)_3)_2(WO_2)_2(BiW_9O_{33})_2]^{10-}$ (**1**), $[(Mn^{II}(H_2O))_3(SbW_9O_{33})_2]^{12-}$ (**2**), and $[(Mn^{II}(H_2O)_3)_2(Mn^{II}(H_2O)_2)_2(TeW_9O_{33})_2]^{8-}$ (**3**) with Standard Deviations

	1	**2**	**3**
W−O_t[a]	1.64(3)−1.79(3)	1.71(2)−1.74(2)	1.70(1)−1.74(1)
W−O_{W2}[b]	1.82(2)−2.11(2)	1.83(2)−2.05(2)	1.85(1)−2.07(1)
W−O_{W3X}[b]	2.16(2)−2.31(2)	2.24(2)−2.37(2)	2.31(1)−2.47(1)
X−O_{W3X}[b,c]	2.10(2)−2.11(2)	1.96(2)−1.97(2)	1.89(1)−1.90(1)
Mn−O_W[b]	2.03(3)−2.11(3)	2.05(2)−2.11(2)	2.08(1)−2.14(1)
Mn−O_{H2}[b]	2.15(3)−2.19(3)	2.11(2)−2.15(3)	2.15(2)−2.25(2)
O−W−O_{cis}	72(1)−104(1)	72(1)−106(1)	70.1(4)−105.2(5)
O−W−O_{trans}	154(1)−174(1)	157(1)−170(1)	153.7(4)−173.6(5)
O−X−O[b,c]	85(1)−88(1)	91(1)−94(1)	89.8(4)−95.5(4)
O−Mn−O_{cis}	80(1)−96(1)	85(1)−91(1)	81.5(4)−97.8(5)
O−Mn−O_{trans}[d]	173(1)	102(1)−106(1)	167.7(5)−178.1(4)

[a] t = terminal. [b] The subscript letters indicate symbols and numbers of bonded neighbor atoms of the oxygens. [c] X = Bi^{III} (**1**), Sb^{III} (**2**), Te^{IV} (**3**). [d] In the case of **2**, O_W-Mn−O_{H2}.

The X-ray structure analysis of the mixed sodium ammonium salt $Na_{11}(NH_4)$[**2**]·$45H_2O$ (Table 1) shows an interesting novel heteropolyanion containing two identical α-B-$[SbW_9O_{33}]^{9-}$ fragments related to each other by a center of inversion and facing each other with their open sites. A belt of three manganese(II) ions connects both defect anions through four oxygen atoms with an average Mn−O_W bond length of 2.08 Å. Each manganese atom has pyramidal coordination including one water molecule (average Mn−O_{H2} bond length 2.13 Å) completing the free site of the manganese cations. In the center of each SbW_9 subunit consisting of three corner-sharing W_3O_{13} groups, the Sb^{III} atom has a distorted ψ-tetrahedral coordination with an average Sb−O_{W3Sb} bond length of 1.96 Å. A view of this interesting cluster is shown in Figure 1b; selected bond lengths and angles are presented in Table 2.

As shown by the crystal structure of Na_8[**3**]·$34H_2O$ (Table 1), the anion **3** is closely related to **1**, also consisting of two identical β-B-$[XW_9O_{33}]^{n-}$ fragments. In contrast to **1**, the central atoms within these subunits are tellurium(IV) atoms pyramidally surrounded by three oxygen atoms with an average Te−O_{W3Te} bond length of 1.90 Å. The second difference is the way the β-B-$[TeW_9O_{33}]^{8-}$ units are connected. They are joined together by two octahedral $Mn^{II}O_4(H_2O)_2$ groups and two $Mn^{II}O_3(H_2O)_3$ octahedra, respectively. The bond lengths are observed between 2.08 and 2.14 Å (Mn−O_w) and between 2.15 and 2.25 Å (Mn−O_{H2}). The structure of **3** is shown in Figure 1c; selected bond lengths and angles are reported in Table 2.

Catalytic Application. Besides their unusual structures, $[(Mn^{II}(H_2O)_3)_2(WO_2)_2(BiW_9O_{33})_2]$,$^{10-}$ $[(Mn^{II}(H_2O))_3(SbW_9O_{33})_2]^{12-}$, and $[(Mn^{II}(H_2O)_3)_2(Mn^{II}(H_2O)_2)_2(TeW_9O_{33})_2]^{8-}$ are

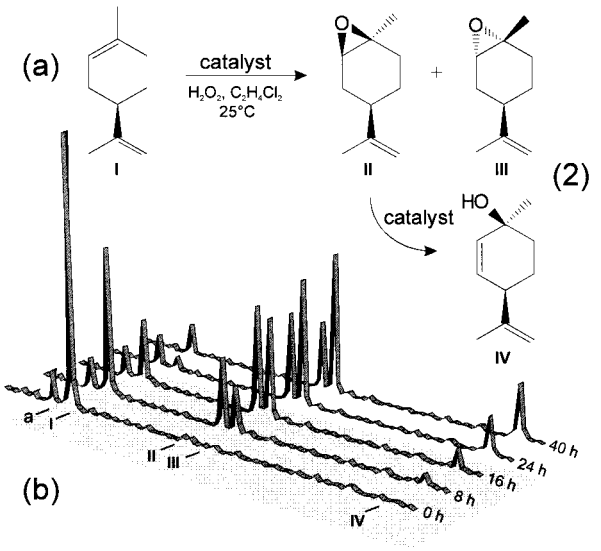

Figure 2. (a) Equation and (b) time-dependent stack GC plot of the regioselective epoxidation of (*R*)-(+)-limonene with hydrogen peroxide exemplified by the use of **1** as a catalyst. Application of **2** and **3** for the same reaction under equal reaction conditions leads to comparable time-dependent GC plots. Reaction conditions: substrate/30%H_2O_2/catalyst = 1000/2000/1, 1,2-dichloroethane as solvent, room temperature. The organic products were analyzed by GC/MS using *p*-cymene (**a**) as an internal standard and ^{1}H NMR spectroscopy. Statements in the Experimental Section give further detailed information on the reaction procedures and product analyses.

remarkably active catalysts for the epoxidation of alkenes. Thus, in a biphasic reaction system (1,2-dichloroethane/water), the model substrate (*R*)-(+)-limonene[26] (**I**) regioselectively reacts with hydrogen peroxide and **1**, **2**, or **3** as a catalyst under aerobic conditions at room temperature to give almost quantitative (with **2**) and high (with **1** and **3**) yields of 1,2-limonene oxide, respectively.

In all cases, both *cis*-1,2-limonene oxide (**II**) and *trans*-1,2-limonene oxide (**III**) were obtained; at first **II** is formed in small excess.[27] During further reaction, **II** partially reacts to give the *cis*-allylic alcohol (**IV**), eq 2 (Figure 2a). The typical development of the product yields as a function of time is presented in Figure 2b.

Importantly, the turnover numbers for the epoxidation of (*R*)-(+)-limonene are very high, and they increase at higher ratios of substrate/oxidant/catalyst at constant reaction time. For example, with a 5000/10 000/1 ratio 2600 (**1**), 2750 (**2**), and 2550 (**3**) turnovers were achieved after 24 h, which is remarkable related to polyoxometalate-catalyzed oxidations of alkenes known from the literature.[16−23] A detailed analysis of the performance of each catalyst as a function of different substrate/oxidant/catalyst ratios at room temperature is given in Table 3. Besides, in first exemplary investigations, much higher turnovers per hour have been achieved at higher temperatures.

Time courses for the oxidation of (*R*)-(+)-limonene with **1**−**3** with a substrate/oxidant/catalyst ratio of 1000/2000/1 at 25 °C as indicated in Figure 3 show conventional behavior due to stable catalyst systems without significant inactivation or inhibition by the products. No induction period or autocatalysis is observed for the generation of the epoxides, while the subsequent production of the alcohol **IV** from **II** indicates such an induction. The achieved yields of *trans*-1,2-limonene oxide (**III**) are almost independent of the applied catalyst and amount to more than 40% after 40 h in each case. Yields of *cis*-1,2-

(26) (*R*)-(+)-Limonene was taken as a model substrate due to its role as a very useful starting material for many organic syntheses, cf.: Szabo, W. A.; Lee, H. T. *Aldrichim. Acta* **1980**, *13*, 13. In qualitative experiments, the epoxidation of another important organic precursor compound, norbornene, under analogous condition with **1** as a catalyst was also successful.

(27) Since no buffer was used during epoxidation of (*R*)-(+)-limonene a fairly acidic pH was maintained in the reaction mixture. Accordingly, the resulting epoxides can be converted to diols which will most likely move preferentially into the aqueous phase containing the hydrogen peroxide reactant. However, this effect is found not to be strong: The internal standard *p*-cymene does not increase appreciably during reaction, and analysis of the organic products gives no hint to this conversion either.

Table 3. Regioselective Epoxidation of (*R*)-(+)-Limonene with Hydrogen Peroxide Catalyzed by $[(Mn^{II}(H_2O)_3)_2(WO_2)_2(BiW_9O_{33})_2]^{10-}$ (**1**), $[(Mn^{II}(H_2O))_3(SbW_9O_{33})_2]^{12-}$ (**2**), and $[(Mn^{II}(H_2O)_3)_2(Mn^{II}(H_2O)_2)_2(TeW_9O_{33})_2]^{8-}$ (**3**)[a]

substrate/oxidant/catalyst ratio	turnover to the products[b] (mmol of products·mmol of cat.$^{-1}$)			
	8 h	16 h	24 h	40 h
1000/2000/1(**1**)	610	890	960	990
2500/5000/1(**1**)	1400	1900	2130	2300
5000/10 000/1(**1**)	2000	2400	2600	3100
1000/2000/1(**2**)	600	760	850	900
2500/5000/1(**2**)	1420	1880	2100	2200
5000/10 000/1(**2**)	1700	2400	2750	3400
1000/2000/1(**3**)	590	720	840	890
2500/5000/1(**3**)	1380	1860	2070	2150
5000/10 000/1(**3**)	1800	2350	2550	3000

[a] Turnover numbers refer to equivalent reaction conditions and different substrate/oxidant/catalyst ratios.[28] Detailed information on the general epoxidation procedure used in all reactions listed in this table is presented in the Experimental Section. [b] Summation of *cis*-1,2-limonene oxide (**II**), *trans*-1,2-limonene oxide (**III**), and *cis*-allylic alcohol (**IV**).

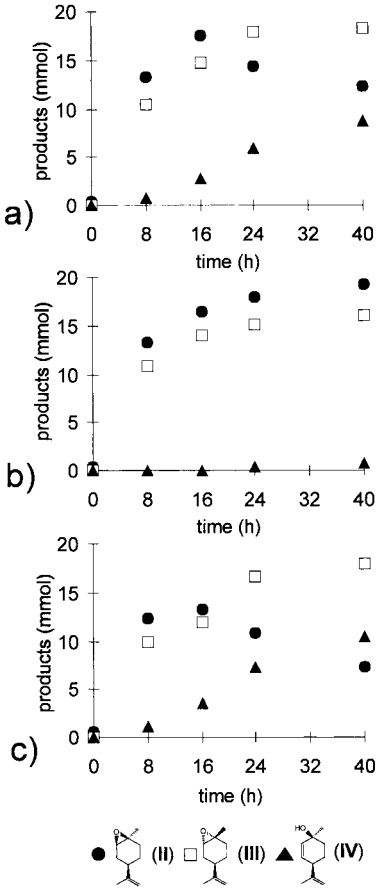

Figure 3. Time-dependent yields of the oxidation products of reaction of 40 mmol of (*R*)-(+)-limonene with 30% hydrogen peroxide (80 mmol) catalyzed by 0.04 mmol of **1** (a), **2** (b), and **3** (c) in 40 mL of 1,2-dichloroethane at room temperature.

Table 4. Distribution of Active Oxygen: Incorporation of Oxygen into (*R*)-(+)-Limonene and Remaining Hydrogen Peroxide[a]

system	organic products[b,d,e] [mmol (%)]	remaining hydrogen peroxide[c,d] [mmol (%)]
without catalyst and substrate	0	64 (80.0)
1 (without substrate)	0	16 (20.0)
2 (without substrate)	0	14 (17.5)
3 (without substrate)	0	12 (15.0)
1	39.6 (49.5)	10 (12.5)
2	36.0 (45.0)	14 (17.5)
3	35.6 (44.5)	7 (8.8)

[a] Reaction conditions: 40 mmol of (*R*)-(+)-limonene with 30% hydrogen peroxide (80 mmol) catalyzed by 0.04 mmol **1**−**3** in 40 mL of 1,2-dichloroethane at room temperature in a biphasic system and 40 h reaction time. [b] Oxygen (mmol) incorporated into (*R*)-(+)-limonene and ((mmoles of oxygen incorporated into (*R*)-(+)-limonene/initial mmoles of hydrogen peroxide) × 100). [c] Hydrogen peroxide (mmol) unreacted and ((mmoles of unreacted hydrogen peroxide/initial mmoles of hydrogen peroxide) × 100). [d] Organic products were analyzed by methods given in the Experimental Section. Hydrogen peroxide was quantified by the titanyl method.[30] [e] Summation of *cis*-1,2-limonene oxide (**II**), *trans*-1,2-limonene oxide (**III**), and *cis*-allylic alcohol (**IV**).

limonene oxide (**II**) after 40 h depend on the catalyst used in the epoxidation process. Application of **2** gives an almost 50% yield of *cis*-1,2-limonene oxide, and use of **1** and **3** as catalysts lead only to a 30% (**1**) and 20% (**3**) yield, respectively, depending on the different tendency of rearrangement of **II** to **IV**. Rates of this conversion for each applied catalyst are also pictorially illustrated in Figure 3.

In this context it is important to point out that in several control experiments the activities of $MnCl_2 \cdot 4H_2O$ and the trivacant polyoxometalate fragments $[XW_9O_{33}]^{n-}$ (X = Bi^{III}, Sb^{III}, Te^{IV}) with H_2O_2 and alkene alone were evaluated and no mentionable turnover numbers were found.[29]

Generally, another fundamental feature of an oxygenation process is the yield of the products based on the oxygen donor. The H_2O_2 efficiency of the investigated epoxidations with **1**−**3** (substrate/oxidant/catalyst ratio = 1000/2000/1) is illustrated in Table 4. Therein, the consumption of the oxygen donor H_2O_2 (active oxygen) is almost 2 times higher than the actual incorporated oxygen, resulting in 49.5% (**1**), 45% (**2**), and 44.5% (**3**) product yields based on hydrogen peroxide, respectively. This effect can be explained by both usual dismutation of H_2O_2 and dismutation of hydrogen peroxide caused by the applied catalysts (eq 3), which is generally the most significant side

$$2H_2O_2 \xrightarrow[\text{(non productive dismutation of active oxygen)}]{\text{transition metal substituted complex}} 2H_2O + O_2 \qquad (3)$$

reaction in transition metal catalyzed hydrogen peroxide based oxygenation of organic substrates[31] and is also observed in the present case. This effect is consistent with the Haber−Weiss peroxide chain breakdown which is often rate-limiting and substantial for most transition metal substituted polyoxoanions.[1] Consumption of the active oxygen is consequently a competition between the epoxidation reaction and the hydrogen peroxide dismutation, both catalyzed by the applied heteropolytungstates **1**−**3**.

To give a more detailed view on the described directed oxygen-transfer process, some additional observations and reflections should be added:

First, it is remarkable that only the trialkyl-substituted double bond within the ring of the substrate is oxidized whereas an oxygenation of the other dialkyl-substituted double bond or simultaneous epoxidation of both double bonds does not occur. This observed regioselectivity is therefore a function of the nucleophilicity of the carbon−carbon double bonds, with increased substitution lowering the necessary activation energies for oxygenation by the catalysts. As a support for this hypothesis the dialkyl-substituted olefin *p*-cymene used as an internal standard was not found to be oxidized by **1**−**3** under equal reaction conditions due to the deficient nucleophilicity of its carbon−carbon double bond. Furthermore, a dependence of the regioselectivity and the product selectivity on temperature or substrate/oxidant/catalyst ratio could not be established: Epoxidation of (*R*)-(+)-limonene under typical reaction conditions with **1**−**3** at 75 °C gives only 1,2-limonene oxide products with almost the same yield of **III** as reaction at 25 °C.

Second, this observed stereoselective conversion may be interpreted as anti-coplanar elimination of the protonized 1,2-limonene oxide depending on the accessibility of the hydrogen atom being in a staggered anti position to the oxyranylic group. As a function of steric hindrance this hydrogen atom can be taken over more easily in the case of **II** by the applied catalysts than in the case of **III** operating as a base. An analogous behavior of **III** could not be observed, and no other theoretically possible products were produced from **I**−**IV**.

Surprisingly, use of **2** as a catalyst leads to a much lower tendency of rearrangement of **II** into **IV** than the applications of **1** and **3**. Furthermore, **IV** was found to be formed more easily at higher substrate/oxidant/catalyst ratios. These observations may be explained by the different basicities of **1**−**3** in the reaction mixtures. Depending on their charges **2** is the most strongly basic anion, followed by **1** and **3**, which was checked by measurement of the pH values of each complex in wet 1,2-dichloroethane: 7.8 (**1**), 8.5 (**2**), and 7.4 (**3**). As a function of concentration **II** can be protonized more easily in case of **3** than in the case of **1**. Application of **2** renders protonation of **II** most effectively due to its highest influence on free protons in the reaction solution. This prevents rearrangement of **II** into **IV**. Importantly, in a control experiment the described conversion of *cis*-1,2-limonene oxide (**II**) to *cis*-allylic alcohol (**IV**) was demonstrated independently by reaction of a *cis*/*trans*-1,2-limonene oxide mixture with **3** in wet acidic 1,2-dichloroethane (pH 6). As expected, in a more acidic solution higher yields of **IV** were achieved besides other products such as diols.

Third, the catalytic properties of **1**−**3** appear to be rather independent from their different structures, numbers of active manganese centers, and free coordination sites; an influence of the different central atoms (Bi^{III}, Sb^{III}, and Te^{IV}) within the XW_9 subunits of each heteropolyanion on catalytic behavior could not be found either. These hypotheses depend on qualitative observations only and need to be clarified, but in fact, the different catalysts achieve almost the same turnover numbers and product selectivities. Probably equal reaction pathways for the epoxidation process are used by the three catalysts.

Another important point is the environmental relevance of the present catalytic systems and the desirable replacement of the organic 1,2-dichloroethane phase with a nontoxic solvent or use of the catalysts in homogeneous chlorocarbon-free media. We tested several different solvents, acetonitrile, acetone, ethanol, and dichloromethane to clarify the catalytic potentials

(28) Reaction rates could differ depending on the purity of the synthesized catalysts.

(29) (*R*)-(+)-limonene/H_2O_2/$MnCl_2 \cdot 4H_2O$, $Na_9[BiW_9O_{33}] \cdot xH_2O$, $Na_9[SbW_9O_{33}] \cdot 19.5H_2O$, and $Na_8[TeW_9O_{33}] \cdot xH_2O$ = 500/1000/1.

(30) DIN 38409-H15 part 1 DEV, Beuth, Berlin.

(31) Cotton, F. A.; Wilkinson, G. *Advanced Inorganic Chemistry*, 5th ed.; Wiley: New York, 1988.

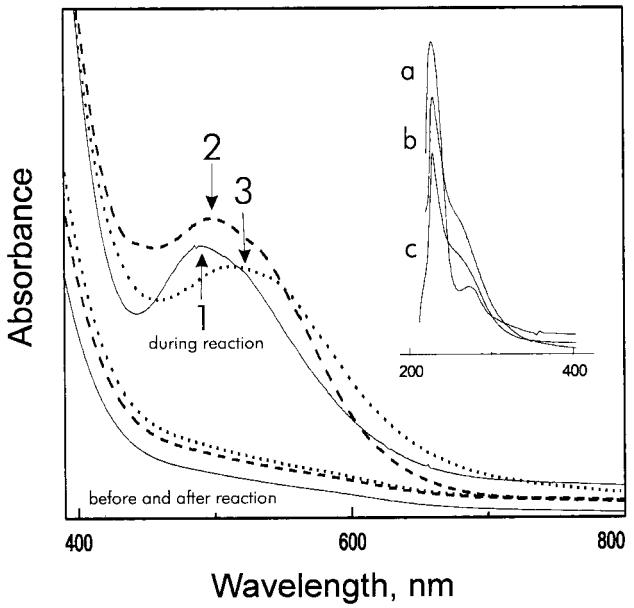

Figure 4. UV−vis spectra of $[(Mn^{II}(H_2O)_3)_2(WO_2)_2(BiW_9O_{33})_2]^{10-}$ (**1**)-(solid lines), $[(Mn^{II}(H_2O))_3(SbW_9O_{33})_2]^{12-}$ (**2**) (dashed lines), and $[(Mn^{II}(H_2O)_3)_2(Mn^{II}(H_2O)_2)_2(TeW_9O_{33})_2]^{8-}$ (**3**) (dotted lines) at different stages of the epoxidation of (*R*)-(+)-limonene in 1,2-dichloroethane: The bottom spectra represent the applied catalysts before and after reaction (several days later) with 2+ oxidation states for the manganese atoms; the top spectra represent the three catalysts during the reaction. The oxidation states of at least one manganese atom of the complexes is changed from 2+ to 3+. Measurement in the 200−400-nm range: (a) methyltricaprylammonium cation, (b) before reaction, and (c) after reaction. Further details are given in the Experimental Section.

of **1**−**3** in these media. Due to insufficient solubility of the catalysts in all cases (except for CH_2Cl_2, similar product rates with **3**), no statement concerning the efficiency of the applied catalysts in chlorocarbon-free media can be made now.

Spectroscopic Measurements. The complete mechanism of the epoxidation reaction remains to be understood in detail;[32] some further features of the process follow from UV−vis, IR, and CV measurements: The oxidation states of the applied catalysts are found to be changed during reaction. Examination of the UV−vis spectra (400−800 nm) of **1**−**3** before, during, and after the epoxidation process (Figure 4) shows at least partially oxidized species $[Mn^{II}_{2-x}Mn^{III}_x(H_2O)_y(WO_2)_2(BiW_9O_{33})_2]^{(10-x)-}$ ($x = 1$ or 2, $0 \le y \ge 6$), $[Mn^{II}_{3-x}Mn^{III}_x(H_2O)_y(SbW_9O_{33})_2]^{(12-x)-}$ ($x = 1-3$, $0 \le y \ge 3$), and $[Mn^{II}_{4-x}Mn^{III}_x(H_2O)_y(TeW_9O_{33})_2]^{8-}$ ($x = 1-4$, $0 \le y \ge 10$). This oxidation of the catalysts, which is indicated by the formation of distinctive peaks at 490 nm (**1**), 498 nm (**2**), and 514 nm (**3**) during reaction to be assigned to d−d electron transitions, is comparable to similar manganese-substituted heteropolyanions used as catalysts in other epoxidation reactions.[16] These observations indicate that the postulated Mn^{III} species play an important role in the epoxidation mechanisms. Probably they are resting states in equilibrium with the true active catalysts which are usually short-lived, present in low concentration, and spectroscopically difficult to detect.

Measurements in the 200−400-nm range before and after reaction show only absorption bands (227 and 273 nm) of the quaternary ammonium salt used for the transfer of the catalysts into the organic phase.

(32) The present paper is not intended to report a detailed analysis of the exact reaction mechanism of the epoxidation process. Results on extensive kinetic and mechanistic studies which are underway will be published soon.

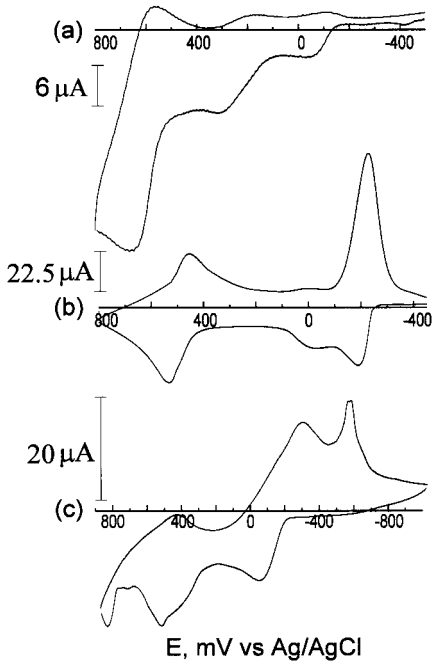

Figure 5. Cyclic voltammogram of $[(Mn^{II}(H_2O)_3)_2(WO_2)_2(BiW_9O_{33})_2]^{10-}$ (**1**), $[(Mn^{II}(H_2O))_3(SbW_9O_{33})_2]^{12-}$ (**2**), and $[(Mn^{II}(H_2O)_3)_2(Mn^{II}(H_2O)_2)_2(TeW_9O_{33})_2]^{8-}$ (**3**) dissolved in 1,2-dichloroethane (1×10^{-3} M). Measurement procedures and electrochemical data for each catalyst are listed in the Experimental Section.

Further support for the importance of the 3+ oxidation state of the manganese centers in each complex during the oxygenation process is obtained from cyclic voltammetric measurements of **1**−**3** (Figure 5). The spectra show comparable electrochemical characteristics of the catalysts indicated by the quasi-reversible one-electron Mn^{2+}/Mn^{3+} oxidation of each anion at ca. 275 mV (**1**), ca. 10 mV (**2**), and ca. 485 mV (**3**) very likely corresponding to a $[Mn^{II}Mn^{II}HPA]-[Mn^{II}Mn^{III}HPA]^+$ redox processes (eq 4). The more anodic waves at ca.

$$\begin{array}{ccc} [Mn^{III}Mn^{III}HPA]^{2+} & \underset{-e^-}{\overset{+e^-}{\rightleftharpoons}} & [Mn^{II}Mn^{III}HPA]^{+} \\ & & \quad -e^- \Big\downarrow \Big\uparrow +e^- \\ [Mn^{II}Mn^{II}HPA]^{-} & \underset{-e^-}{\overset{+e^-}{\rightleftharpoons}} & [Mn^{II}Mn^{II}HPA] \end{array} \qquad (4)$$

([$Mn^{II}Mn^{II}$HPA] = **1**, **2**, **3**)

640 mV (**1**), ca. 480 mV (**2**), and ca. 840 mV (irreversible oxidation, probably resulting from slow electron-transfer rather than chemical irreversibility) (**3**) can be assigned to the formation of $[Mn^{III}Mn^{III}HPA]^{2+}$. These main features of the voltammograms agree with similar observations reported for manganese(II)-substituted heteropolyanions with Mn^{2+}/Mn^{3+} redox potentials of ca. 200 mV and ca. 450 mV,[16] 500 mV,[33] and 710 mV,[33] respectively. The cathodic waves at ca. −80 mV (**1**), ca. −130 mV (**2**), and ca. −140 mV (**3**) imply that each of the complexes can be electrochemically reduced corresponding to the formation of $[Mn^{II}Mn^{II}HPA]^-$; for **3**, another (irreversible) reduction observed at ca. −580 mV.

Finally, the solvolytic stability of the applied catalysts is an important point: Generally, polyoxometalates are thermodynamically and oxidatively stable compounds. Though they are known to be degraded in some cases by aqueous hydrogen

(33) Zhang, X.-Y.; Pope, M. T.; Chance, M. R.; Jameson, G. B. *Polyhedron* **1995**, *10*, 1381−1392.

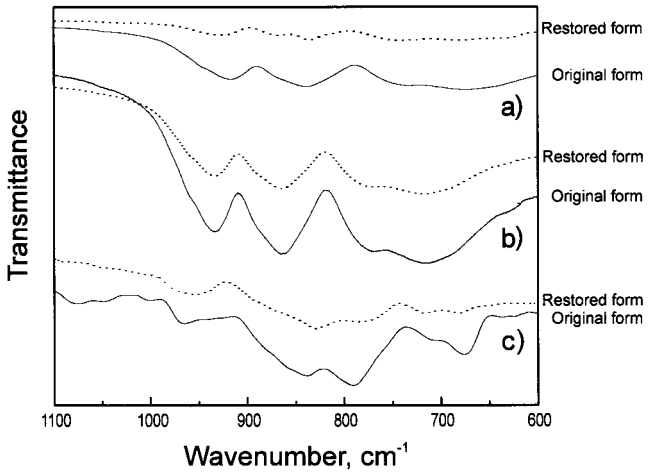

Figure 6. IR spectra of $[(Mn^{II}(H_2O)_3)_2(WO_2)_2(BiW_9O_{33})_2]^{10-}$ (**1**) (a), $[(Mn^{II}(H_2O))_3(SbW_9O_{33})_2]^{12-}$ (**2**) (b), and $[(Mn^{II}(H_2O)_3)_2(Mn^{II}(H_2O)_2)_2(TeW_9O_{33})_2]^{8-}$ (**3**) (c) before (solid lines) and after reaction, restored to their original form (dotted lines), indicating the stability of each catalyst during the epoxidation process. Details are presented in the Experimental Section.

peroxide[34] **1**−**3** seem to be stable under the oxidative conditions found in a typical epoxidation procedure.

This hypothesis is supported by the following arguments: After being treated with hydrogen peroxide in a typical reaction after 990 (**1**), 900 (**2**), and 890 (**3**) turnovers, the IR spectra of the applied catalysts (Figure 6, showing the important wavenumber area for W−O−W vibrations from 1100 to 600 cm^{-1}) are almost unchanged due to their stability during reactions. Details on the observed vibrations with corresponding wavenumbers are reported in the Experimental Section.

(34) Aubry, C.; Chottard, G.; Platzner, N.; Brégeault, J.-M.; Thouvenot, R.; Chaveau, F.; Huet, C.; Ledon, H. *Inorg. Chem.* **1991**, *30*, 4409−4415.

In addition to this, UV−vis spectra of **1**−**3** show only the original anions in oxidized forms during reaction and the primary compounds several days after completion of the epoxidations after 990 (**1**), 900 (**2**), and 890 (**3**) turnovers. Furthermore, no indications of degradation of $[(Mn^{II}(H_2O)_3)_2(WO_2)_2(BiW_9O_{33})_2]^{10-}$, $[(Mn^{II}(H_2O))_3(SbW_9O_{33})_2]^{12-}$, and $[(Mn^{II}(H_2O)_3)_2(Mn^{II}(H_2O)_2)_2(TeW_9O_{33})_2]^{8-}$ were observed in the course of the catalytic reactions.

Conclusion

The novel manganese(II)-substituted heteropolyanions, $[(Mn^{II}(H_2O)_3)_2(WO_2)_2(BiW_9O_{33})_2]^{10-}$, $[(Mn^{II}(H_2O))_3(SbW_9O_{33})_2]^{12-}$, and $[(Mn^{II}(H_2O)_3)_2(Mn^{II}(H_2O)_2)_2(TeW_9O_{33})_2]^{8-}$, are highly efficient and stable catalysts for the epoxidation of dienes. In the case of the model substrate (*R*)-(+)-limonene they achieve almost quantitative regioselectivities with exclusive oxygenation of the more nucleophilic carbon−carbon double bond. Importantly, the epoxidation processes can be performed at ambient temperatures with high turnover numbers and low consumption of hydrogen peroxide. Studies are in progress that address the energetic and mechanistic features of these remarkable catalytic reactions covering also other anions of the same types with different transition metals.

Acknowledgment. This work was supported by the Deutsche Forschungsgemeinschaft, the Fonds der Chemischen Industrie, and the Hoechst AG, Corporate Research & Technology.

Supporting Information Available: Further details of the X-ray investigation, tables of positional and thermal parameters, and thermal ellipsoid figures for $Na_6(NH_4)_4$[**1**]·$37H_2O$, $Na_{11}(NH_4)$[**2**]·$45H_2O$, and Na_8[**3**]·$34H_2O$ (9 pages, print/PDF). The Crystallographic Information File (CIF) can be downloaded from the Internet; see any current masthead page for ordering information and Internet access instructions.

JA974281V